

# 3

INJURY SCIENCE RESEARCH  
Proceedings of the Twenty-Eighth International Workshop

## A Method for the Study of Close-Proximity Occupant-Air Bag Interactions

F. A. Bandak, P. C. Chan, K. H. Ho and Z. Lu

### ABSTRACT

*An experimental Air Bag Test System (ATS) to study air bag-occupant interactions during close proximity deployment has been developed. It serves as a research tool to study controllable and repeatable air bag deployments. The ATS was calibrated to replicate target response due to an arbitrarily selected air bag inflator type. A mathematical model was developed to describe the ATS deployment with favorable validation. The model follows an integral approach that treats the unfolding of the bag during deployment as a uniform thinning surface with specified volume-area functions. The model was used to explain the test data and provide insight into the effects of energy partition during a deployment including the effects of varying inflator temperature and vent holes on target load. The ATS and the model were used to generate benchmark data for computational model and code development validations. Test and modeling studies were performed for one air bag type and are extendable to a wide variety of fleet air bags. Results provided insights on the effects of inflation energy and mass flow on target response. They show that only a very small fraction (3%) of the total deployment energy is delivered to a target, while 60% is stored in the air bag. For a sealed bag, the target response is independent of inflator temperature if the total energy is held constant. Venting reduces the target load primarily during the final pressurization (membrane) phase. For a vented bag, the target velocity decreases with higher inflator temperature.*

### INTRODUCTION

Air bags are designed to inflate rapidly to cushion the impact of an occupant during a car crash. Air bag inflation can create large mechanical forces that can injure out-of-position (OOP) occupants by exerting high loading on the chest, abdomen, and head/neck regions (Patrick and Nyquist, 1972; Sullivan et al., 1992; Lau et al., 1993; Mertz et al., 1995; Yoganandan et al., 1995; Johnston et al., 1997). Previous static, sled, and crash test data have shown that there is a wide variation in dummy responses to air bag loads. Loads from the same air bag on test dummies can change significantly with small variation of dummy positions (Horsch et al., 1990; Melvin et al., 1993; Bass et al., 1999). Static tests using different air bags have also shown a wide variation of impact load on the same-size dummy at the same position relative to the air bag (Pilkey, 1996a, 1996b). There exists little phenomenological explanation for this variation.

A standardized test method that provides complete information on the air bag, target, and bag-target interaction is not available. An efficient and repeatable laboratory test method is needed to systematically explore the factors affecting the air bag-target interaction, while providing a technique of standardized comparison of existing and proposed air bags. Recent work by Duma et al. (1997) attempted to use a pneumatic deployment system as a laboratory study method but the reported results were limited to only reproducing air bag tip velocities that were still too low and no target impact tests were done. Current procedures provide dummy response data, and some limited information of the geometric and gas dynamics effects of the air bag itself. Little data is gathered on loading. Recent work by Nusholtz et al. (1998 and 1999) indicates the importance of relating the target response to inflation characteristics. An understanding of the relation between the air bag inflation characteristics and the resultant load and occupant responses will help evaluate future, proposed air bag modifications.

Air bag-occupant deployment interactions have been studied using mathematical models. These models can be classified into two categories 1) multi-body rigid models, and 2) finite element models. Multi-body models assume a series of pre-selected shapes for the air bag without describing the details of the unfolding process. They have the advantage of computational simplicity and hence can be used to conduct parametric design studies (Wang and Ngo, 1990; Deng and Wang, 1994; and Deng, 1995). Nusholtz and co-workers (1998, 1999) included the integral effect of energy flow rate and heat transfer in their multi-body model studies. Several air bag studies using finite elements yielded qualitative results (Wawa et al., 1993; Tanavde et al., 1997). Applications ranged from frontal thoracic impacts (Lin et al., 1995, Digges, et al., 1997, and Plank et al., 1998), head injury (Ruan and Prasad, 1994), and interaction with out-of-position child (O'Connor and Rao, 1992, Sieveka et al., 1999), to the study of bag unfolding details (Wawa et al., 1993, Tanavde et al, 1997, and Vaidyaraman et al. 1998).

The objective of this work is to: 1) develop a laboratory ATS to evaluate air bag load under controllable and repeatable inflation conditions; 2) develop an integral lumped-parameter analytical model coupling the bag inflation to target response to help understand the fundamental parameters controlling the inflation-occupant load relationships; 3) use the ATS as a research tool to study air bag deployment dynamics and bag-dummy interactions particularly for small occupants in OOP conditions; and 4) to generate benchmark data sets complete enough for code and computational model development validations.

## METHODS

### Air Bag Test System

A reusable, pneumatically-driven ATS was constructed to provide repeatable deployment using the same air bag. The schematic of the ATS design is shown in Figure 1. The ATS gas source is a high-pressure reservoir (Figure 1) made of polyvinyl chloride (PVC) pipe with a 7.5-in. inner diameter, which is pressurized by laboratory compressed air. The air bag, without the inflator, is attached to the exit pipe of the reservoir (Figure 1). An aluminium rupture diaphragm, separating the air bag from the reservoir, is punctured by a gas-driven plunger to initiate inflation. The reservoir pressure, volume, and rupture diaphragm size can be adjusted to control the inflation characteristics. The diaphragm rupture technique more closely simulates the pyrotechnic gas generation rate than the use of an electromechanical control valve, such as that used by Horsch et al. (1990) and Melvin et al. (1993). Duma's (1997) pneumatic-activation method for valve opening resulted in air bag tip velocity that were considered low compared to the fleet air bags.

Two rigid targets were used for impact studies. The mid-size target is an aluminium cylinder with a diameter of 12" (30.5 cm) and a mass of 77-lb (35-kg), representing a 50<sup>th</sup> percentile adult male upper body. The small target is also an aluminium cylinder but with a diameter of 10" (25.4 cm) and a mass of

59 lb (27 kg), representing a small (5<sup>th</sup> percentile) adult female upper body (Figure 1). The target is hinge-mounted at the top and the proximity of the target to the air bag can be adjusted (Figure 2).

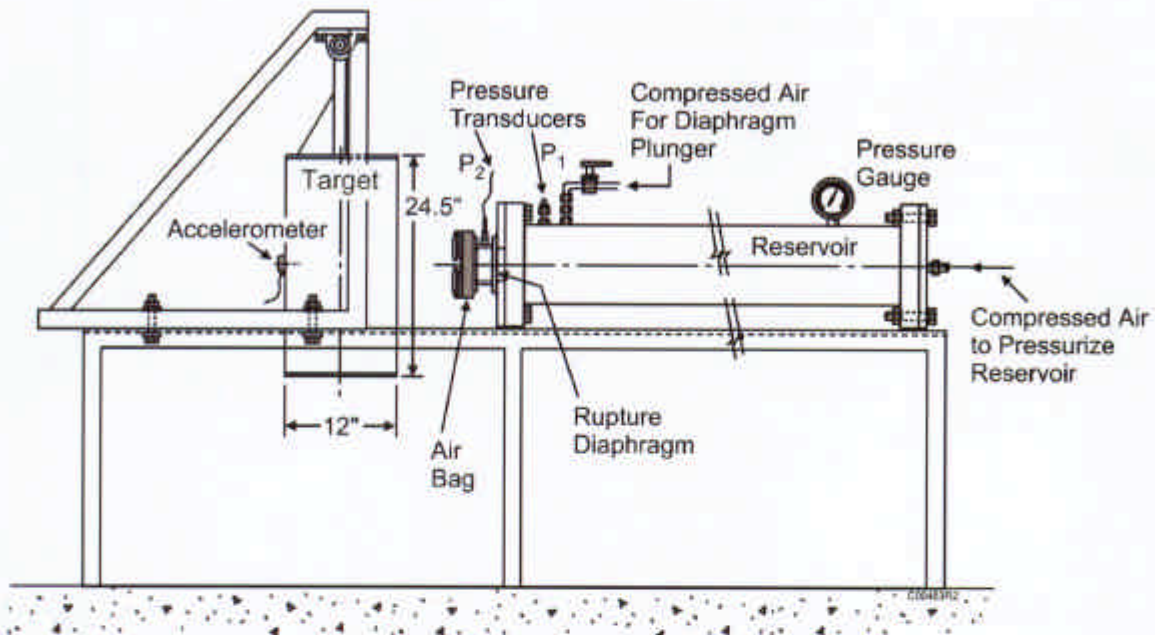
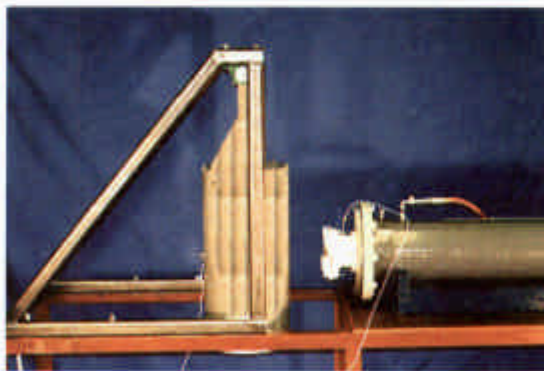
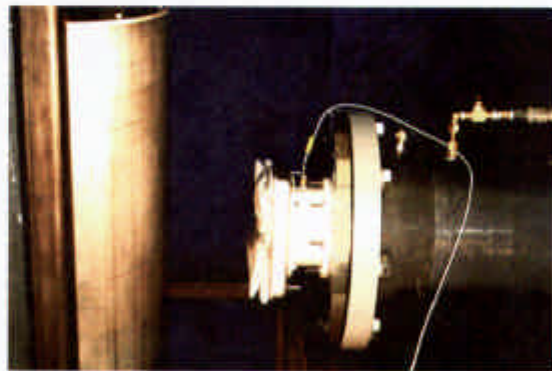


Figure 1. Schematic of ATS fixture.



(a) Far view



(b) Close view

Figure 2. Air bag test setup with target standoff at 4 in.

The ATS was instrumented to measure air bag inflation characteristics and target response. Pressures on both sides of the rupture diaphragm were measured, providing pressure differentials for mass flow rate calculations. The pressure downstream of the diaphragm ( $P_2$ ) is taken to be the air bag pressure (Figure 1). Air bag and reservoir pressures were measured using Endevco Piezoresistive Transducers, Models 8510B and 8530C, with an Endevco DC Amplifier, Model 136. An Endevco Accelerometer, Model 7251A-10, with a PCB Signal Conditioner, Model 483A, is mounted on the back of the target to

measure the whole body acceleration. Data were recorded on a PC with a National Instruments Dynamic Signal Acquisition Board (AT-A2150) with a data-sampling rate of 5 kHz and were analyzed using LabView 4.0. High-speed movies are taken to observe air bag opening interactions with the target.

#### Calibration of the ATS against Fleet Air Bag Inflator (Igniter)

The ATS was calibrated against an air bag inflator by adjusting parameters to adequately replicate target response. The procedure follows four steps: 1) characterize the air bag inflator energy output using the sealed tank test, 2) measure the target response due to the inflator, 3) set the ATS reservoir pressure to match the inflator energy output, and 4) adjust the ATS orifice size and fine tune reservoir pressure to match the target response dynamics with the inflator

*Society of Automotive Engineers standard tank test.* The Society of Automotive Engineers (SAE) standard tank test was used to characterize the selected air bag inflator. The tank is a sealed hollow cylinder with 19.75" (50.2 cm) diameter and 12" (30.5 cm) depth and has a volume of 60 L as specified in SAE J2238 (1995). The inflator is separated from the air bag unit, connected to the tank, and electrically discharged. The tank gas pressure and temperature histories are then recorded as shown by the gauge locations in Figure 3.

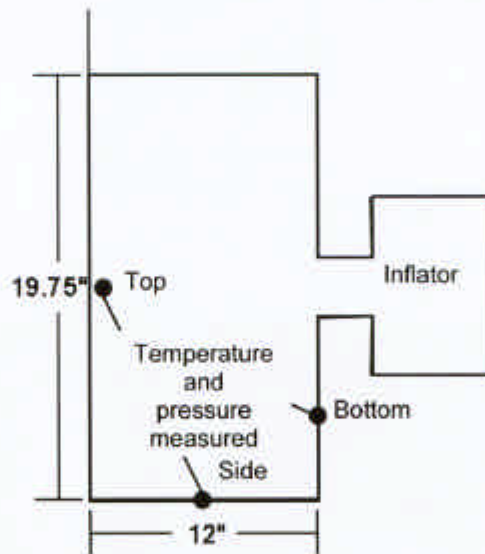


Figure 3. Schematic of inflator tank test with instrumentation indicated.

Using the gas pressure and temperature recorded from the tank test, the instantaneous energy stored in the tank,  $E_T$ , can be calculated as

$$E_T = MC_v T_T \quad (1a)$$

and using ideal gas law,

$$E_T = \frac{P_T V_T}{\gamma - 1} \quad (1b)$$

where  $P_T$  is the tank gas pressure,  $V_T$  the tank volume,  $T_T$  the tank gas temperature,  $M$  the gas mass in the tank,  $C_v$  the constant volume specific heat, and  $\gamma (= C_p/C_v)$  the ratio of specific heats (with  $C_p$  being the constant pressure specific heat). The pyrotechnic inflator combustion process produces a gas mixture that is mostly nitrogen with specific heat ratio  $\gamma$  close to that of air and was taken as constant at 1.4. We

assumed an adiabatic process and the energy discharged from the inflator,  $E_i$ , is equal to the energy stored in the tank,  $E_T$ :

$$E_i = E_T = \frac{P_T V_T}{\gamma - 1} \quad (2)$$

and the energy flow rate is

$$\dot{E}_i = \frac{dE_i}{dt} = \frac{V_T}{\gamma - 1} \frac{dP_T}{dt} \quad (3)$$

Eq. (2) shows that the tank pressure,  $P_T$ , is an indicator of the inflator energy,  $E_i$ . The total gas mass discharged from the inflator  $M_i$  is equal to the mass lost by the inflator,

$$M_i = M_{i1} - M_{i2} = \frac{E_i}{C_p T_i} \quad (4)$$

where  $M_{i1}$  and  $M_{i2}$  are the mass of the inflator measured before and after the tank test, respectively. Assuming the inflator temperature is constant during deployment,  $T_i$  can be calculated from Eq. (4) as

$$T_i = \frac{E_i}{C_p M_i} \quad (5)$$

The inflator mass flow rate is then given by

$$\dot{M}_i = \frac{\dot{E}_i}{C_p T_i} \quad (6)$$

Since the tank temperature is also measured, Eq. (1a) can be used to verify the measured inflator mass output, which is used for model calculations for the inflator.

The ATS reservoir pressure  $P_R$  is set to match the inflator energy,

$$P_R = \frac{E_i(\gamma - 1)}{V_R} \quad (7)$$

where  $V_R$  is the reservoir volume. This energy matching is based on the principle that equal work on the target should be obtained from equal energy. This, however, is only a static equivalence since it does not address deployment dynamics. Dynamic tuning is performed by adjusting the orifice diameter so that the target response due to the ATS matches the inflator. Minor tuning of the reservoir pressure is necessary to replicate the full dynamics of the actual air bag deployment by the inflator. An adapter bracket was added to the exit pipe to measure the target response due to the inflator. The inflator was initiated by an electrical signal synchronized with the target accelerometer triggering. When the inflator deploys the air bag, no pressurization of the ATS reservoir is needed. Four driver side air bags were studied this way. These were taken from the National Highway Traffic Safety Administration (NHTSA) OOP test series and are designated Bag A, UVA384, UVA386, and TC3067. Tank and impact tests were performed for all four inflators and Bag A was used for ATS calibration and further proximity studies for the present work.

### **Integral Analytic Model**

An analytic model was formulated based on a lumped-parameter approach (Figure 4). Figures 4a and b show the early and intermediate stages of the air bag-target interaction. Figure 4c shows the chest-thorax component that will be described later. The pressure in the bag was taken to be uniform in space, but varying in time. The bag, with mass  $M_B$ , was represented by a membrane of uniform density, whose

surface area,  $A$ , and surface mass density,  $\sigma$ , vary with time. The shape of the bag is arbitrary. The surface mass density is given by

$$\sigma = \frac{M_B}{A} \quad (8)$$

An equation relating the volumetric expansion of the air bag and the motion of the target was derived using integral approach. We first consider the normal motion of a surface element,  $ds$ , with velocity  $v_n$  in the free part of the bag (Figures 4a-b):

$$\frac{d}{dt}(v_n \sigma ds) = (p_B - p_A) ds \quad (9)$$

where  $p_B$  and  $p_A$  are the gas pressure in the ambient atmosphere and in the bag, respectively. As shown in Figure 4a-b, only a fraction of the bag surface with area  $A_c$  touches and moves with the target while the rest expands freely. Integrating Eq. (9) over the free bag surface elements results in an equation relating the change of the air bag volume  $V$  to the acceleration of the target and the pressure difference across the bag surface. The detailed derivation is presented in Appendix A with the final equation given as follows:

$$\frac{d}{dt} \left( \sigma \frac{dV}{dt} \right) - \sigma A_c \frac{d^2 x_c}{dt^2} = (A - A_c)(p_B - p_A) \quad (10)$$

where  $x_c$  is the position of the target (Figure 4). The second term in Eq. (10) accounts for the rate of volumetric change of the part of the bag moving together with the target. The model solves for the air bag volume  $V$  and the target position  $x_c$  coupled with the air bag pressure  $p_B$ , with the deployment provided by the ATS or an inflator. The model requires the specification of the total bag surface area,  $A$ , and the target contact area  $A_c$ . The surface area,  $A$ , and the target contact area,  $A_c$ , were computed as functions of the instantaneous air bag volume,  $V$ , and the target position,  $x_c$ . Functional forms that are bounded by the initial and fully deployed characteristics of the air bag with parameters that can be varied to describe the intermediate unfolding process were selected. Before the bag is deployed, it contains the initial gas volume,  $V_0$ , and initial surface area,  $A_0$ . When it is fully inflated as free deployment, the maximum air bag volume is  $V_1$  and the maximum surface area is  $A_1$  and the front of the bag will have traveled the maximum distance  $x_B$ . The parameters  $V_0$ ,  $A_0$ ,  $V_1$ ,  $A_1$ , and  $x_B$  were determined based on the observed starting and ending configurations of an air bag during free deployment. The air bag was assumed to have a simple geometry at all time to establish volume-area functions. The bag surface area  $A$  is modeled as a linear function of the bag volume  $V$

$$\frac{A - A_0}{A_1 - A_0} = \begin{cases} \frac{1}{\xi} \frac{V - V_0}{V_1 - V_0} & , \quad 0 < \frac{V - V_0}{V_1 - V_0} < \xi \\ 1 & , \quad \xi < \frac{V - V_0}{V_1 - V_0} \end{cases} \quad (11)$$

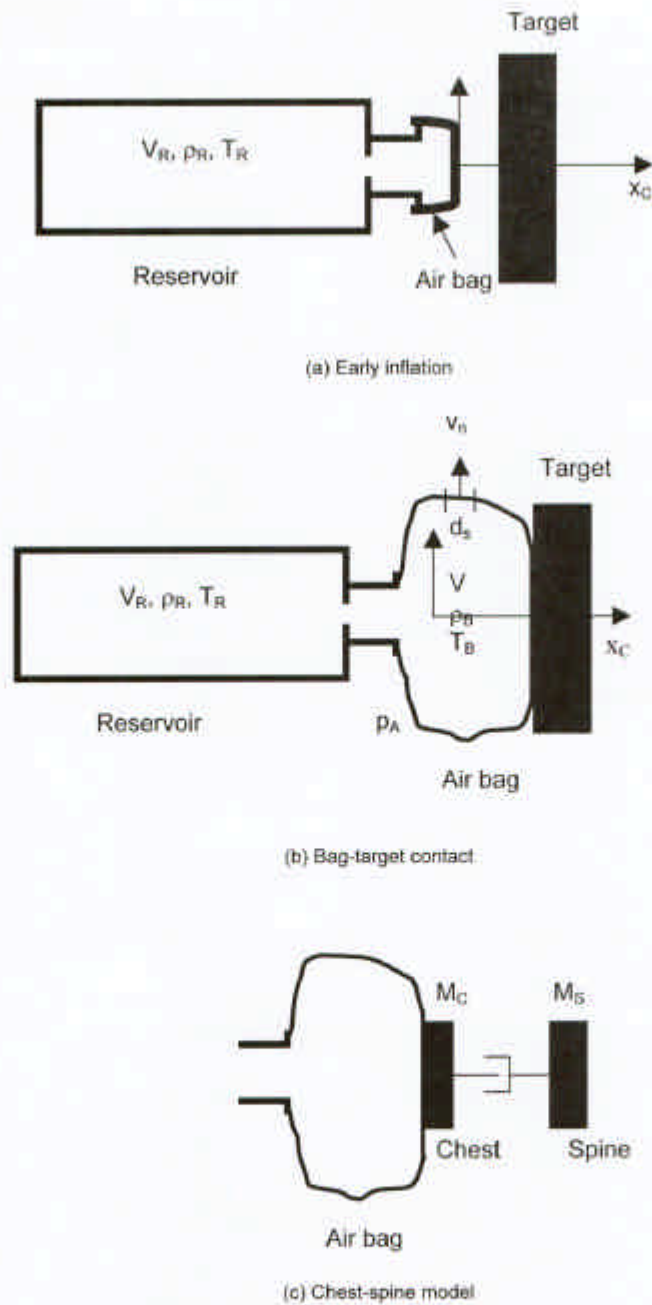


Figure 4. Air bag-target model.

where  $\xi$  ( $\sim 0.3$ ) is a parameter that can be determined by data calibration possibly with the help of high-speed movie analysis of the air bag unfolding process. Figure 5 shows an example of the area-volume function [Eq. (11)] in dimensional form used for Bag A. It can be changed for different air bags. Since the bag can only unfold during deployment, we impose the condition that  $A$  can only increase with time

$$\frac{dA}{dt} \geq 0 \quad (12)$$

A minimum volume criterion is needed to determine whether the bag is in contact with the target at different positions. Under non-zero standoff, there is a time delay for the bag to touch the target, and under violent conditions, the target may also separate momentarily from the air bag. The minimum contact volume,  $V_{C,min}$ , of the air bag at which target contact occurs is defined as a simple linear function of the target position,

$$V_{C,min} = V_0 + (\theta V_f - V_0) \frac{x_c}{x_0}, \quad 0 < \frac{x_c}{x_0} < 1 \quad (13)$$

where  $\theta$  (-0.25) is a parameter that can be determined from data calibration. Figure 6 shows an example for Eq. (13) for Bag A (together with the maximum volume function explained later). When the air bag volume  $V \geq V_{C,min}$ , there is bag-target contact, but  $V$  is not allowed to exceed its limit  $V_{max}$  that is also a function of target position.

A relationship governing the maximum bag volume  $V_{max}$  versus target position  $x_c$  is needed. As shown in Figure 6, the  $V_{max}$  function consists of a linear portion for  $x_c < x_0$  and a nonlinear portion for  $x_c > x_0$ , where  $x_0$  is a parameter determined for a specific air bag. When the target obstructs the bag, the maximum volume attained by the bag can be lower than the free maximum volume  $V_f$ . For  $x_c > x_0$ , the air bag shape is approximated as an ellipsoid with semi-axes  $b$  and  $a$  (Figure 7). The axes are calculated from the observed volume  $V_f$  of the fully deployed bag, with the axis ratio,  $b/a$ , estimated from the high-speed movie. When the air bag is in contact with the target, it is assumed that the bag takes on a partial ellipsoidal volume with a flat front interface with the target (Figure 7). For the nonlinear portion,  $x_0 \leq x_c \leq x_B$ , the maximum bag volume,  $V_{max}$ , is

$$V_{max} = \frac{2}{3} \pi b^2 a + \pi b^2 \left( \tau - \frac{\tau^3}{3a^2} \right) \quad (14a)$$

$$\tau = a_0 + (a - a_0) \frac{(x_c - x_0)}{(x_B - x_0)}, \quad x_0 \leq x_c \leq x_B$$

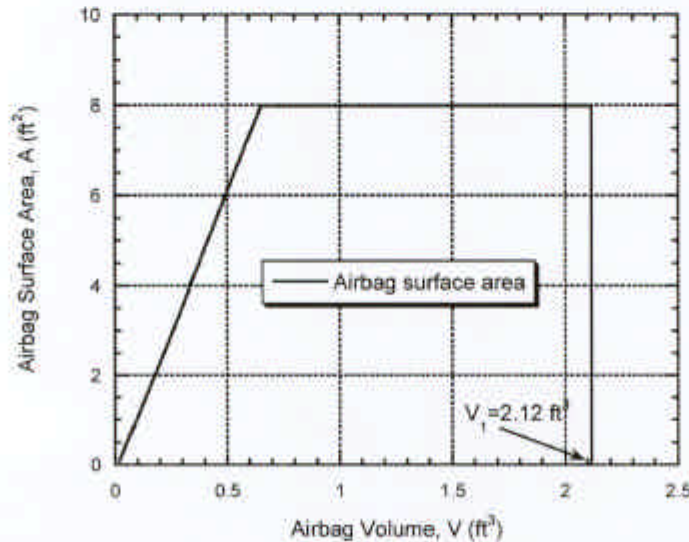


Figure 5. Air bag surface area function.

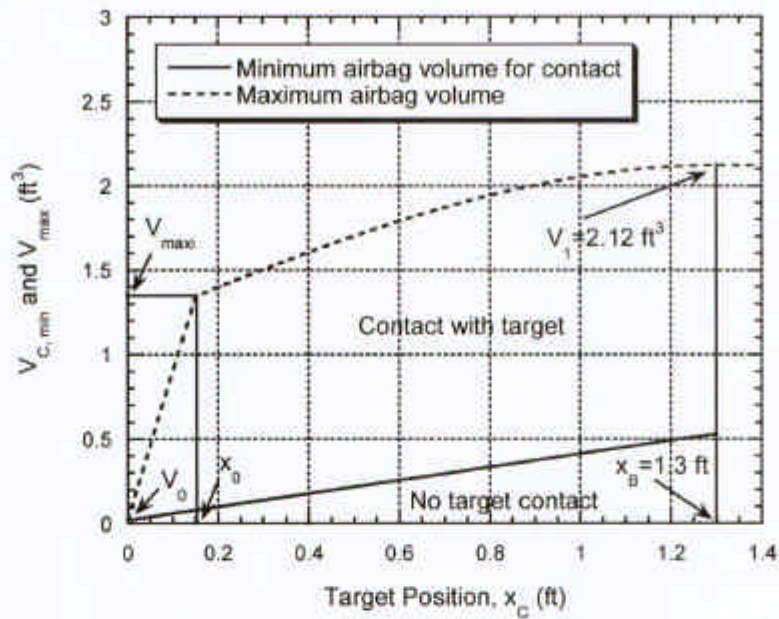


Figure 6. Minimum air bag volume for contact and maximum bag volume.

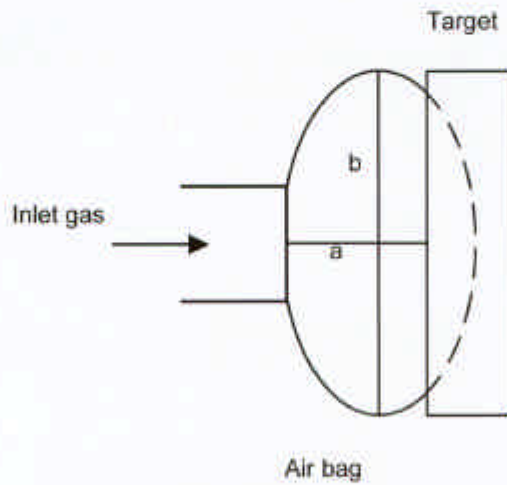


Figure 7. Ellipsoidal approximation of air bag shape.

where  $a_0$  ( $-a \leq a_0 \leq a$ ) is a parameter determined by data fitting and  $\tau$  is an auxiliary variable (Figure 6). From Eq. (14a), when  $x_c = x_b$ ,  $\tau = a$ , the final maximum bag volume is equal to  $V_1 = (4/3) \pi b^2 a$ . If  $x_c = x_0$ ,  $\tau = a_0$ , we have the intermediate maximum volume,  $V_{max}$ ,

$$V_{max} = \frac{2}{3}\pi b^2 a + \pi b^2 \left(a_0 - \frac{a_0^3}{3a^2}\right) \quad (14b)$$

which joins the lower linear portion at  $x_0$  (Figure 6). For the linear portion,  $0 \leq x_c \leq x_0$ , a linear function connects the initial bag volume,  $V_0$ , to the intermediate maximum volume  $V_{max}$  (Figure 6),

$$V_{max} = V_0 + (V_{max} - V_0) \frac{x}{x_0}, \quad 0 \leq x \leq x_0 \quad (15)$$

Eqs. (14)-(15) provide a complete specification of the maximum bag volume versus target position, as illustrated in Figure 6 for Bag A.

Fabric stretching due to overpressure can increase the bag volume. To account for this effect, the maximum volume calculated from Eqs. (14) or (15) is increased to

$$V'_{max} = \left[1 + \frac{3(1-2\nu)(a+b)}{4Et} (P_B - P_A)\right] V_{max} \quad P_B > P_A \quad (16)$$

where  $t$  is the bag fabric thickness,  $E$  the Young's modulus, and  $\nu$  the Poisson's ratio of fabric material.

#### Compatibility Condition and Contact Area

To determine the air bag-target contact area, we derive a relationship between the air bag volume and the contact area. During the air bag deployment process, only a part of the bag is in contact with the target. Consequently, the total bag volume increase  $\Delta V_{total}$  is divided into two parts,

$$\Delta V_{total} = \Delta V_{contact} + \Delta V_{free} \quad (17)$$

where  $\Delta V_{contact}$  is the volume increase from the movement of the surface that is in contact with the target, and  $\Delta V_{free}$  is the volume increase from the free surface movement (Figure 4). Since the bag can only unfold during deployment,  $\Delta V_{total}$ ,  $\Delta V_{contact}$  and  $\Delta V_{free}$  are positive most of the time. Then an inequality equation can be imposed as

$$\Delta V_{total} \geq \Delta V_{contact} \quad (18)$$

Note that

$$\Delta V_{contact} = A_c \Delta x_c \quad (19)$$

where  $\Delta x_c$  is the incremental displacement of the target (Figure 4). Combining Eqs. (18) and (19), an inequality relationship between the contact area and volume change rate is obtained as

$$A_c \leq \frac{\Delta V_{total}}{\Delta x_c} \quad (20)$$

Eq. (20) should be satisfied whenever contact area and/or volume functions are chosen; otherwise, energy conservation may not be satisfied in the numerical calculation. It is a compatibility condition governing the geometry consistency or deformation compatibility.

To satisfy the deformation compatibility condition, we use the equality in Eq. (20) to find the contact area from the maximum bag volume function [Eqs. (14)-(16)] as

$$A_c = \frac{\Delta V_{max}}{\Delta x_c} \quad \text{but} \quad A_c \leq A_{c,max} \quad (21)$$

where  $A_{c,max}$  is the maximum contact area determined by the specific air bag and target geometry. The importance of calculating the contact area this way is that whenever the maximum volume function is changed, the compatibility condition is always satisfied so that energy conservation is observed. Figure 8

shows an example of the contact area function for Bag A, where the contact area increases rapidly to  $A_{c,max}$  and gradually decreases to zero as the bag inflates and pushes the target away.

### Air Bag Gas Dynamics

The gas inside the air bag is supplied by the inflow mass flux  $f_m$  from the ATS or the inflator and depleted by mass flux,  $f_{leak}$ , through the vent holes and/or fabric leakage. Assuming that the pressure and density of the gas inside the bag is uniform, the equation for the conservation of mass is:

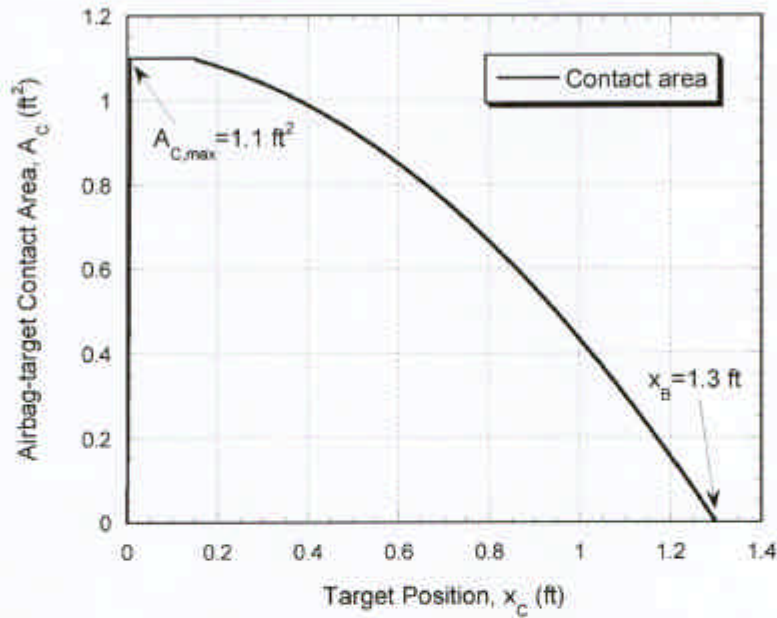


Figure 8. Air bag-target contact area function.

$$\frac{d}{dt}(V\rho_B) = f_m - f_{leak} \quad (22)$$

where  $\rho_B$  is the density of the gas inside the bag. Let  $T_B$  be the temperature of the gas inside the bag and  $e_m$  be the inflow energy per unit mass. The change of internal energy of the gas in the bag is

$$\frac{d}{dt}(\rho_B V c_v T_B) = f_m e_m - f_{leak} C_p T_B - P_B \frac{dV}{dt} - Q \quad (23)$$

where  $Q$  is the heat loss through the bag surface. For the fast process of bag deployment, we assume  $Q = 0$ , and the gas behaves as an ideal gas

$$P_B = \rho_B R T_B \quad (24)$$

For gas flow through the vent holes and the bag porosity with a lumped leak area  $A_{leak}$ , the mass flux is given by

$$f_{leak} = \left\{ \begin{array}{l} C_D A_{leak} \sqrt{\gamma P_B P_B} \left( \frac{\gamma+1}{2} \right)^{\frac{\gamma+1}{2(\gamma-1)}}, \quad P_B \geq P_A \left( \frac{\gamma+1}{2} \right)^{\frac{\gamma}{\gamma-1}} \\ C_D A_{leak} \sqrt{\gamma P_B P_B} \sqrt{\frac{2}{\gamma-1} \left[ \left( \frac{P_A}{P_B} \right)^{\frac{\gamma-1}{\gamma}} - 1 \right] \left( \frac{P_A}{P_B} \right)^{\frac{\gamma+1}{\gamma}}}, \quad P_B < P_A \left( \frac{\gamma+1}{2} \right)^{\frac{\gamma}{\gamma-1}} \end{array} \right\} \quad (25)$$

where  $C_D$  and  $C'_D$  are the drag coefficients,

### ATS Reservoir Model

For the ATS, a gas reservoir model is used to deploy the air bag. With the assumption that the pressure and density of the gas in the reservoir is uniform, the equation for the conservation of mass is

$$V_R \frac{d}{dt} \rho_R = -f_m \quad (26)$$

where  $\rho_R$  is the density of the gas in the reservoir. Let  $T_R$  be the temperature of the reservoir, then the change of internal energy of the reservoir is given by

$$\frac{d}{dt} (\rho_R V_R C_v T_R) = -f_m e_m \quad (27)$$

The mass and energy fluxes are given by

$$f_m = \left\{ \begin{array}{l} C_D A_e \sqrt{\gamma P_R P_R} \left( \frac{\gamma+1}{2} \right)^{\frac{\gamma+1}{2(\gamma-1)}}, \quad P_R \geq P_B \left( \frac{\gamma+1}{2} \right)^{\frac{\gamma}{\gamma-1}} \\ C_D A_e \sqrt{\gamma P_R P_R} \sqrt{\frac{2}{\gamma-1} \left[ \left( \frac{P_B}{P_R} \right)^{\frac{\gamma-1}{\gamma}} - 1 \right] \left( \frac{P_B}{P_R} \right)^{\frac{\gamma+1}{\gamma}}}, \quad P_R < P_B \left( \frac{\gamma+1}{2} \right)^{\frac{\gamma}{\gamma-1}} \end{array} \right\} \quad (28)$$

$$e_m = c_p T_R \quad (29)$$

The density and pressure of the gas in the reservoir is related by the ideal gas law

$$P_R = \rho_R R T_R \quad (30)$$

### Gas Impingement Model

A gas impingement load is added to the target due to the high velocity gas exit from the reservoir. Assuming that the gas pressure downstream of the orifice represents the air bag pressure, the Mach number at the orifice exit,  $M_e$ , is calculated as

$$M_e = \sqrt{\frac{2}{\gamma-1} \left[ \left( \frac{P_B}{P_R} \right)^{\frac{\gamma-1}{\gamma}} - 1 \right]} \quad (31)$$

The gas density at the orifice exit is

$$\rho_e = \rho_R \left( 1 + \frac{\gamma-1}{2} M_e^2 \right)^{\frac{1}{\gamma-1}} \quad (32)$$

where  $\rho_R$  is the upstream reservoir gas density. Then the gas velocity at the exit is

$$V_e = M_e \sqrt{\gamma \frac{P_R}{\rho_e}} \quad (33)$$

The gas jet from the reservoir is similar to a stagnating flow impingement on the target. Based on momentum conservation over the control volume surrounding the jet and the target surface, the gas impingement force  $F_e$  on the target is

$$F_e = \rho_e V_e^2 A_e \quad (34)$$

where  $A_e$  is the orifice area. This impingement load from Eq. (34) is added to the regular contact force  $A_C (P_B - P_A)$  as the total force applied to the target. The impingement load is important especially during the early deployment phase.

### Inflator Model

To simulate the air bag inflator, its energy flow rate and mass flow rate are obtained from the calibration tank tests, which are used as inputs in Eqs. (22) and (23) to deploy the bag. For an adiabatic tank, conservation of energy relates the energy from the inflator,  $E_i$ , and the energy stored in the tank,  $E_T$  according to Eq. (2). The inflator energy and mass flow rates are calculated using Eqs. (3) and (6), respectively,

$$f_m e_{in} = \frac{dE_i}{dt} = \frac{V_T}{\gamma-1} \frac{dP_T}{dt} \quad (35)$$

$$f_m = \frac{V_T}{\gamma-1} \frac{dP_T}{dt} \frac{1}{C_p T_i} \quad (36)$$

### Thorax Response Model

The target can be modified as a chest-thorax model to evaluate chest injuries due to impact load (Figure 4c). The thorax model is based on previous work by Lobdell (1972) for solid impactors and Stuhmiller et al. (1996, 2000) for air blast loading on the chest. As shown in Figure 4c, the model consists of a chest mass,  $M_C$ , coupled to a spine mass,  $M_S$ , by a damper with damping coefficient  $C$ . Denote the positions of  $M_C$  and  $M_S$  by  $x_C$  and  $x_S$ , respectively. The equation of motion of the chest is then

$$\left( M_C + \frac{A_C}{A} M_B \right) \frac{d^2 x_C}{dt^2} = A_C (P_B - P_A) - C \left( \frac{dx_C}{dt} - \frac{dx_S}{dt} \right) \quad (37)$$

where  $A_C M_B/A$  is the mass of the bag in contact with the chest. The equation of motion for the spine is then

$$M_S \frac{d^2 x_S}{dt^2} = C \left( \frac{dx_C}{dt} - \frac{dx_S}{dt} \right) \quad (38)$$

This model is not used for the present effort but is presented for completeness.

**Simulations and Model Parameters**

The model was used to analyze the tests conducted for Bag A, including tank tests, ATS calibration tests and proximity studies. The same set of air bag volume-area functions was used for all calculations. The model was validated against the test data. Theoretical studies were performed to understand the inflation energy partitioning, vent hole effects and inflator temperature effects. The following tables list the parameters and their values used in the simulation for Bag A. Most of the parameters related to a specific air bag (Table 2) need to be modified if a different bag is simulated.

Table 1. Physical Parameters.

Symbol	Units	Value	Definition
$P_a$	KPa	101.3	Atmospheric pressure
$R$	J/kg <sup>o</sup> K	287.5	Gas constant
$C_v$	J/kg <sup>o</sup> K	2.51R	Specific heat at constant volume
$C_p$	J/kg <sup>o</sup> K	$C_v + R$	Specific heat at constant pressure
$\gamma$	-	$C_p / C_v$	Ratio of specific heats

The model parameters physically determined for Bag A are  $A_0 = 0.08 \text{ ft}^2$  (74.3 cm<sup>2</sup>),  $A_1 = 7.98 \text{ ft}^2$  (0.74m<sup>2</sup>),  $V_1 = 2.12 \text{ ft}^3$  (0.06 m<sup>3</sup>), and  $M_0 = 0.569 \text{ lb}$  (0.259 kg). Based on the observed free bag inflation, the maximum bag travel distance  $x_B$  is set to 1.3-ft (0.396 m).

**RESULTS**

**Tank and Impact Tests for Inflators**

Tank tests and target impact tests were performed for four inflators: Bag A, UVA384, UVA386, and TC3067 (Figure 9). These inflators were selected because previous NHTSA data were available. All four inflators were purchased in 2000. All air bags except for Bag A are tethered, and they all vary in size and vent hole designs (Figure 9). These four inflators and air bags were deployed into the same tank and against the same small target, successively, without the covers.

As shown in Figure 10, considerable variations in the tank and impact responses were observed for the four air bags. The tank pressures for the four inflators vary from 21 to 30 psi, with UVA386 showing the weakest rise rate as well as peak pressure (Figure 10a). Bag A and TC3067 produce almost identical (and the highest) tank pressure of 30 psi, as well as the highest tank temperatures of 300-330<sup>o</sup>C (Figure 10a-b). UVA386 and UVA384 produce similar tank temperatures of about 240<sup>o</sup>C (Figure 10b).

Although the TC3067 and Bag A inflators produce the same tank pressures, they inflate their air bags to produce widely different target loads and responses (Figure 10a, c, d). The peak target velocities for Bag A and TC3067 are 22 and 7.5 ft/s, respectively (Figure 10c). Bag A produces a peak target velocity three times as TC3067, as Bag A produces a much stronger second acceleration pulse from 10-50 ms (Figure 10c-d). These data confirm that sealed tank tests are not adequate for evaluating air bag deployment dynamics and potential hazards.

Table 2. Air Bag Parameters.

Symbol	Units	Value	Definition
$M_B$	kg	0.259	Mass of air bag
$A_{leak}$	cm <sup>2</sup>	13.5	Area of leak (including vent holes and fabric leak)
$C_D$	-	0.72	Drag coefficient under choked flow conditions
$C_{D0}$	-	0.72	Drag coefficient under unchoked flow conditions
$V_0$	cm <sup>3</sup>	566.3	Volume of air in bag before deployment
$A_0$	cm <sup>2</sup>	74.3	Area of bag before deployment
$V_1$	m <sup>3</sup>	0.06	Volume of air in bag when deployed
$A_1$	m <sup>2</sup>	0.74	Area of bag when deployed
$X_B$	cm	39.6	Maximum displacement of air bag front when fully deployed
$A_{c,max}$	m <sup>2</sup>	0.167	Maximum area of contact of air bag with target
$a_0$	-	0.18a	Parameter controlling $V_{max}$
$\zeta$	-	0.3	Parameter controlling $A$

Table 3. Reservoir Parameters.

Symbol	Units	Value	Definition
$V_R$	cm <sup>3</sup>	$3.62 \times 10^4$	Volume of pressurized reservoir
$A_0$	cm <sup>2</sup>	Varied	Area of inlet nozzle
$T_R(0)$	°K	300	Initial reservoir temperature
$P_R(0)$	kPa	Varied	Initial reservoir pressure

Table 4. Target Parameters.

Symbol	Units	Value	Definition
$M_C$	kg	34.9 or 28.6	Mass of target (mid-size or small)
$M_S$	kg	0	Mass of spine (not used)
$C$	kg/s	0	Damping coefficient of thorax (not used)

Bag A was selected for further study using the ATS. The air bag module has the bag folded inside an aluminium holder covered by a plastic cover with precut rupture grooves, with a solid propellant inflator (igniter) mounted at the base. The inflator and air bag were separated and used for ATS calibration and proximity tests. The bag was mounted to the ATS exit pipe for deployment by the ATS against a target (Figure 2). After a test, the bag was refolded by hand following the original pattern and held together by tape for another deployment. A single bag can be used more than 50 times.

### **ATS Calibration against Bag A Inflator**

The ATS reservoir pressure and the orifice size are two key parameters controlling the inflation characteristics and target response. Their effects are demonstrated by parametric tests varying the pressure and orifice size successively, where limited repeat tests for each condition were also conducted to quantify data spread. The small target was used at 0-standoff. Figure 11 shows that when the orifice size was kept constant at 2.5" the target velocity increases with the reservoir pressure with minimal timing change. Note that test data are presented with the test numbers preserved in parentheses. When the reservoir pressure was kept constant (50 psi), the target velocity peaks earlier and higher with increasing orifice size (Figure 12). Figs. 11-12 show that the target response can vary by 10-20% under the same conditions, which is not uncommon for air bag tests.

The ATS was calibrated against the Bag A inflator by adjusting the reservoir pressure and orifice size following the procedure described in Section 2, [Eqs. (1)-(7)]. The small target was used at 0-standoff. Based on energy equivalence [Eq. (7)], the ATS reservoir pressure should be 47 psi, and target response timing was tuned by the orifice size. The final ATS reservoir pressure and orifice diameter were fine tuned to be 45 psi and 3.5" respectively to replicate the dynamic response of the target, as shown in Figure 13. The calibrated reservoir pressure (45-psi) is within 5% of that suggested by energy equivalence (47 psi). The target velocity and timing as well as acceleration were well reproduced by the ATS (Figure 13). The acceleration data show that the bag-target interaction is practically finished in 60 ms (Figure 13b). Therefore, the slight divergence between the target velocities beyond 60 ms is immaterial for load considerations (Figure 13a). An example of high-speed movie record for an ATS deployment is shown in Figure 14, where only approximate times can be indicated. The calibration test demonstrates that the ATS can be calibrated to reproduce the target response due of a specific air bag inflator type.

### **Model Validation**

The integral model was first validated against the Bag A inflator tank and impact data. The recorded inflator tank pressure as shown in Figure 10a was used in Eqs. (3) and (6) for energy and mass inflow inputs to the model. The calculated tank pressure and temperature agree well with the data (Figure 15-16). Some minor temperature fluctuations were observed probably due to flow turbulence inside the tank (Figure 16). The target velocity response was well reproduced by the model within 10% (Figure 17), where it should be understood again that the bag-target interaction is practically over in 60 ms. The favorable data comparison validates the modeling of the inflator for the integral model.

The model was further validated against the ATS calibration test data for Bag A. The calculated reservoir and bag pressures agree with the data (Figure 18). The model overpredicts the target peak velocity by about 5%, which is considered well within the data spread (Figure 19). The calculated target acceleration also compares favorably with the data as shown in Figure 20. These results validate the gas dynamics and flow coefficients used in the model. More data comparison and discussion of the relationship between inflation characteristics and target response are presented in the next section.

### **Proximity Tests**

Proximity tests were conducted using the ATS to study target response as a function of standoff from the air bag. The reservoir volume was 1.28 ft<sup>3</sup> (0.036 m<sup>3</sup>) with an initial pressure of 65 psi (448 kPa) and an orifice diameter of 2.5". The mid-size target was used with standoff varying from 0 to 10". Model calculations were performed to explain the data and understand the relationship between bag-target interaction and inflation characteristics. Bag A was used for repeat deployments by the ATS.



Figure 9. Photographs of air bags studied.

The change of inflation characteristics with standoff can be understood from the pressure data as shown in Figure 21 together with the model calculations. After diaphragm rupture, the reservoir pressure decreases almost linearly and merges with the bag pressure at about 90 ms, after which both pressures decrease slowly to zero as a result of venting. The measured reservoir pressure shows a stepwise decrease feature due to the reflections of the rarefaction wave initiated at diaphragm rupture (Figure 21). The observed reservoir stepwise wave period is about 8 ms, which is close to the acoustic wave period of the reservoir with a length of 4.15 ft (1.27 m) and sound speed of 1000 ft/s (304 m/s). Nevertheless, the observed air bag pressures indicate no pulsation effects, probably due to strong turbulent dissipation. The calculated reservoir pressures agree with the data for all three standoffs (Figure 21). Pressure data were highly repeatable.

The air bag pressure data show that the bag generally deploys in three phases: (1) early inflation from about 0-10 ms, (2) intermediate overexpansion from 10-30 ms, and (3) final pressurization from 30-70 ms, (Figure 21). A strong punch-out spike for all three standoffs characterizes the early inflation phase, but the pressure peak and duration are the strongest for 0-standoff (Figure 21). When the target standoff is zero, the initial expansion of the bag is hindered not only by the mass of the bag but also the target. This leads to stronger bag pressure build up that results in a higher and wider punch out pressure pulse when compared to non-zero standoff deployments (Figure 21). From 10-30 ms, there is a period of low

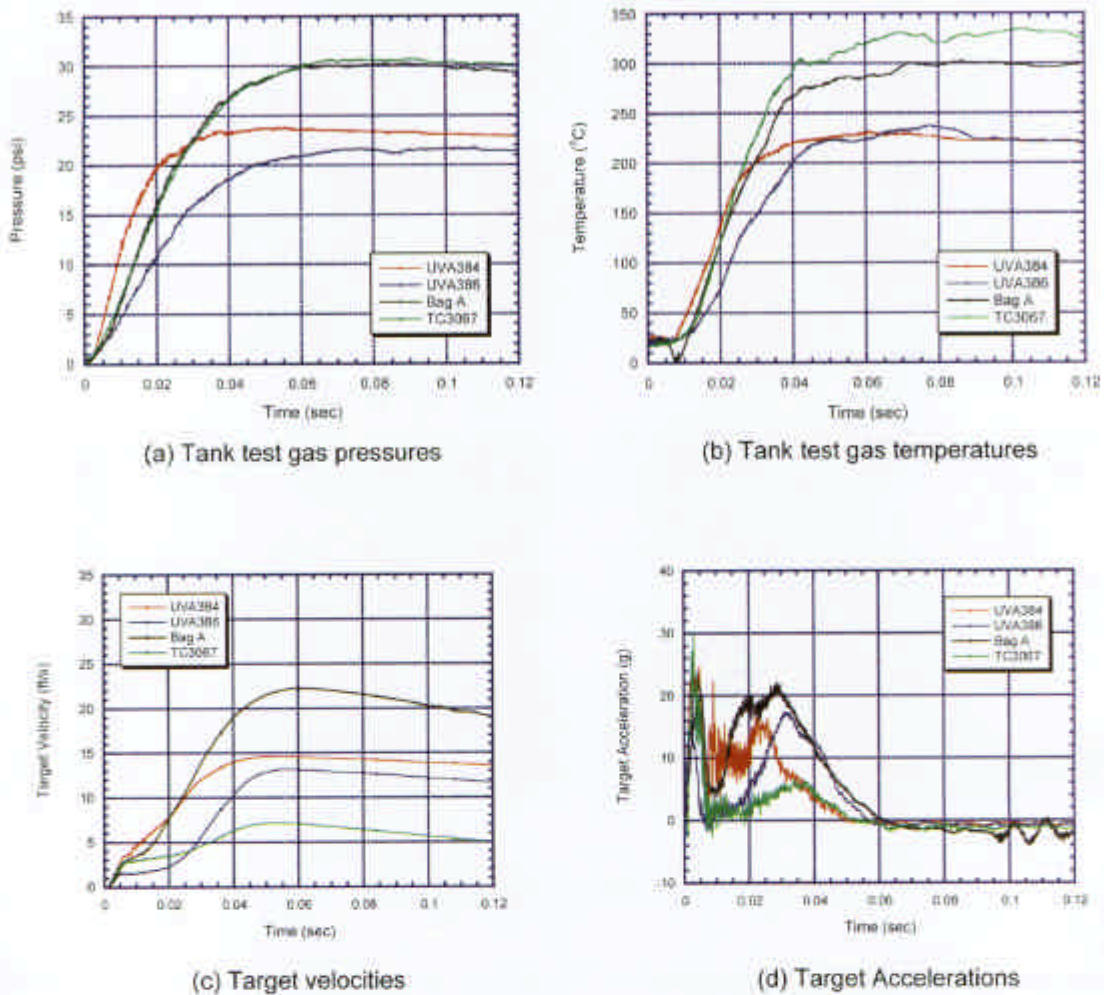


Figure 10. Inflator tank and impact test data.

pressure, which indicates an overexpansion phase with the bag expanding faster than the gas inflow, probably due to the high bag momentum developed during the early inflation phase. When the gas flow catches up at about 30 ms, the pressure rises again to a final peak of about 6-psi before venting eventually brings the gas pressure back to ambient. The final pressurization peaks at 40 ms at 0-standoff but delays to 70 ms at 10-in. standoff. The three-phase trend of the air bag pressure produced by the ATS agrees with the description in SAE J1630 (1995). The observed early inflation phase and the final pressurization phase generally correspond to the punch-out and membrane load phases, respectively, as suggested by Melvin et al. (1993). The early punch-out load is expected to be a significant factor for OOP hazard considerations.

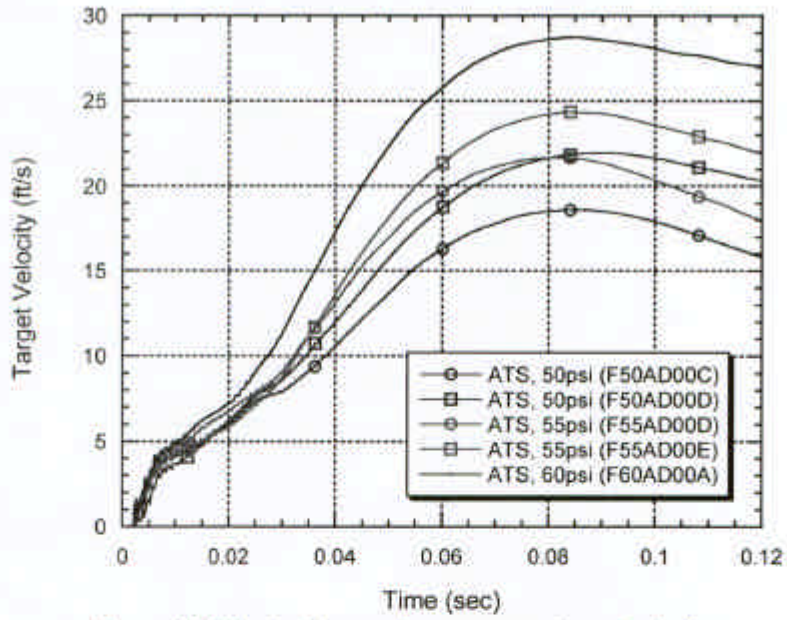


Figure 11. Effects of reservoir pressure on target velocity.

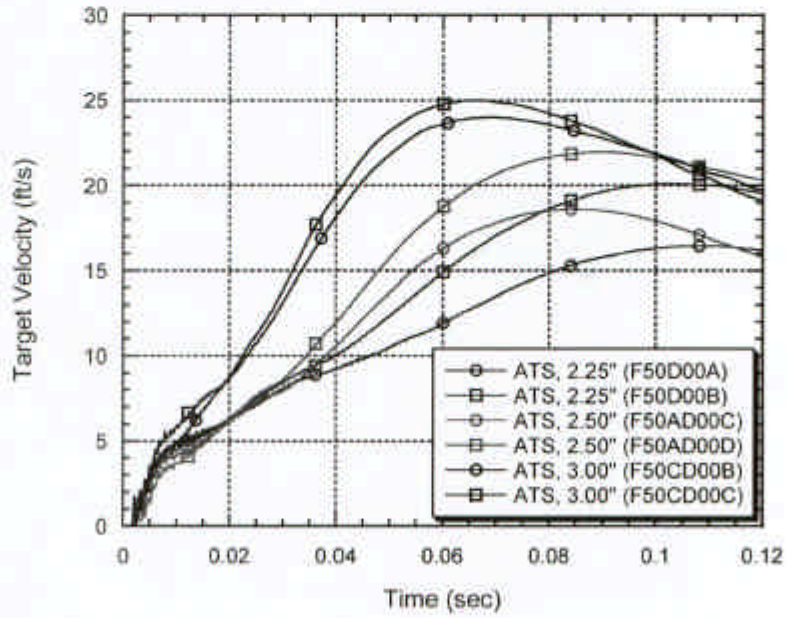
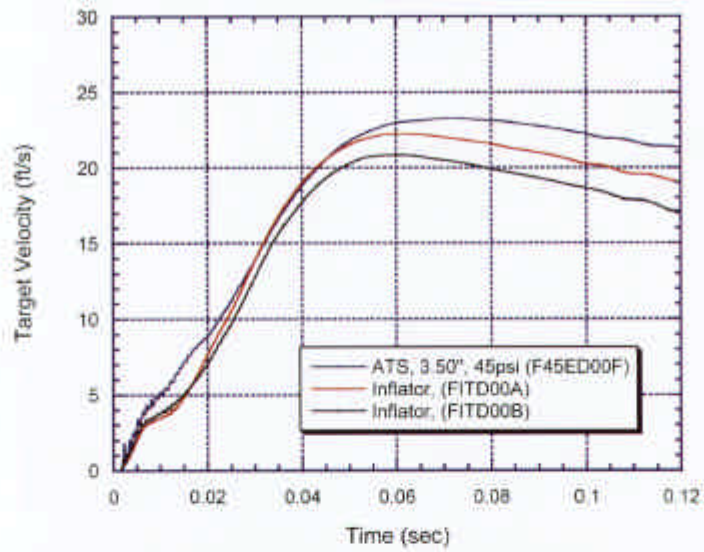
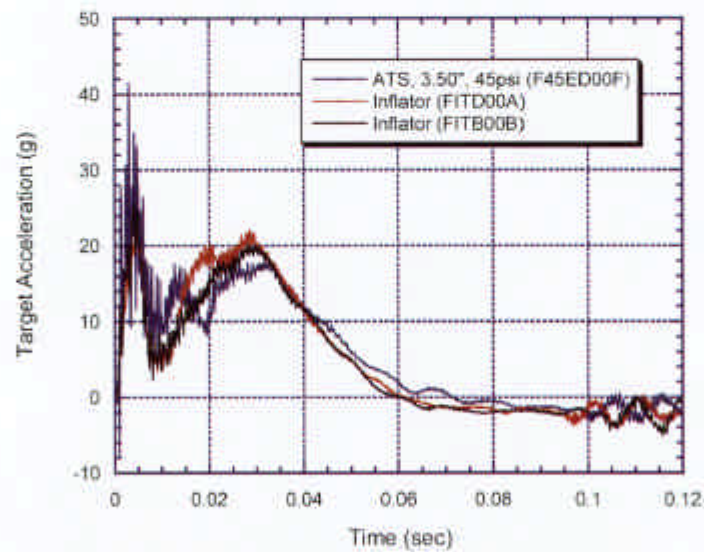


Figure 12. Effects of reservoir orifice size on timing and target velocity.



(a) Target velocity data comparison: ATS vs. inflator



(b) Target acceleration data comparison: ATS vs. inflator

Figure 13. ATS calibration against Bag A inflator.

Proximity tests show that the overall weakening of air bag pressure with standoff correlates with the reduction of target velocity (Figure 21-22). Increasing the standoff from 0 to 10" reduces the early punch out load, extends the intermediate overexpansion phase, and slows down the final pressurization (membrane) load (Figure 21). In contrast to 0-standoff, the target at 4" and 10" contacts less with the air bag during early inflation from 0-10 ms (Figure 21b, c). In fact, the velocity data indicate that the bag does not touch (accelerate) the target at 4" and 10" standoff until at about 5 ms when the target starts to move ( $\Delta v > 0$ ) (Figure 22b, c). When contact begins at around 5 ms, the bag enters the overexpansion phase with low pressure. Consequently, compared to 0-standoff, early OOP load is reduced significantly for 4" and 10" standoff, as confirmed by the significant target velocity reduction from 0-20 ms in Figure 22. On the other hand, the peak target velocity only drops slightly (~10%) from 0" to 4" standoff but by 60% from 4 to 10" standoff (Figure 22). Therefore, there is significant early OOP load reduction from 0-4" standoff, while overall load reduction from 4-10" standoff is primarily due to lower membrane load.

The calculation results compare favorably with the pressure and target data (Figure 21-22). The model captures the early inflation pressure pulse at 0" standoff but overpredicts it by about 35% for 4" and 10" standoff (Figure 21), which could be due to the uncertainty in bag volume during early expansion. The model seems to overpredict the bag pressure during the intermediate overexpansion from 10-30 ms for 4" and 10" standoff (Figure 21b, c). However, it is likely that the pressure gauge ( $P_2$ ) downstream of the orifice understates the bag pressure during this supersonic overexpansion phase since the gauge may be too close to the orifice (Figure 1). In particular, Figure 22b-c indicate that the target velocity continues to increase from 5-30 ms, meaning load is applied to the target, which seems to be unlikely if the bag sustains a significant underpressure as suggested by Figure 21b-c. The sudden pressure jump at about 30 ms at the end of the intermediate overexpansion is likely due to a shocking process commonly seen from an overexpanded jet with downstream obstruction (Figure 21b-c). The model predicts essentially zero-pressure during the intermediate overexpansion and the target is accelerated primarily by gas impingement (Figure 21b, c). It is expected that the final pressurization pressure beyond 30 ms should be accurately measured under subsonic flow condition. The target velocities are well predicted by the model (Figure 22).

#### **Energy and Inflator Temperature Effects Analysis**

The calculated results for the calibrated ATS deployment were analyzed to understand the partition of energy from the deployment at 0-standoff (Figure 23). Analysis shows that about 60% of the energy is stored in the bag, 25% is used for expanding the bag, 15% is lost through venting and leakage, but only 3% is used for moving the target (Figure 23).

Calculated results suggest that since only a small fraction (3%) of the total energy is delivered to the target, precise load control may not be an easy task. Consideration of this result has an impact on the use of energy reduction methods, such as depowering or multistaging, to reduce OOP hazard. The relationship between inflator energy reduction and energy delivered to the target under various conditions needs to be well understood. It seems that many parameters can easily and significantly change the energy delivered to the target (occupant), such as due to bag folding, venting, bag impact angle, gas properties and other compartment conditions during crash. During a crash situation, sufficient energy must be assured to inflate the bag within the required time window for effective occupant protection and this must not be compromised by over-reduction of inflator energy. Furthermore, with only 3% of energy delivered to the target, it is not unusual to observe significant target response data variations.

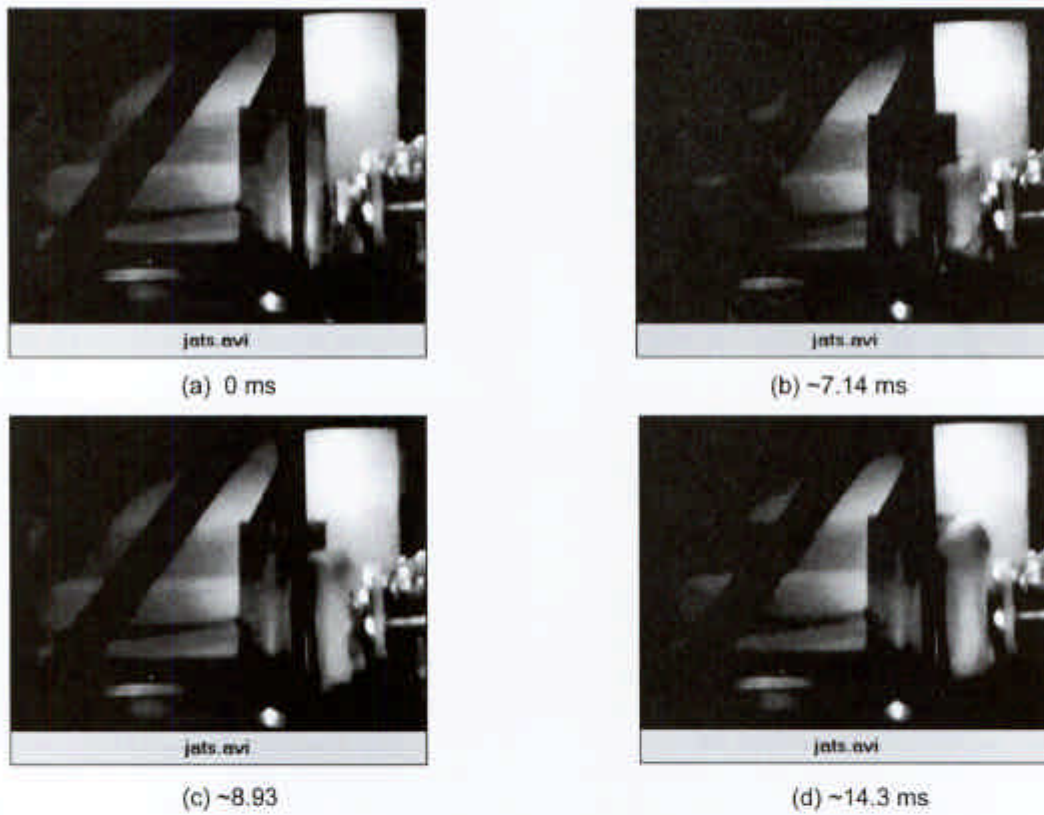


Figure 14. Example of high-speed movie of ATS deployment (1680 fps).

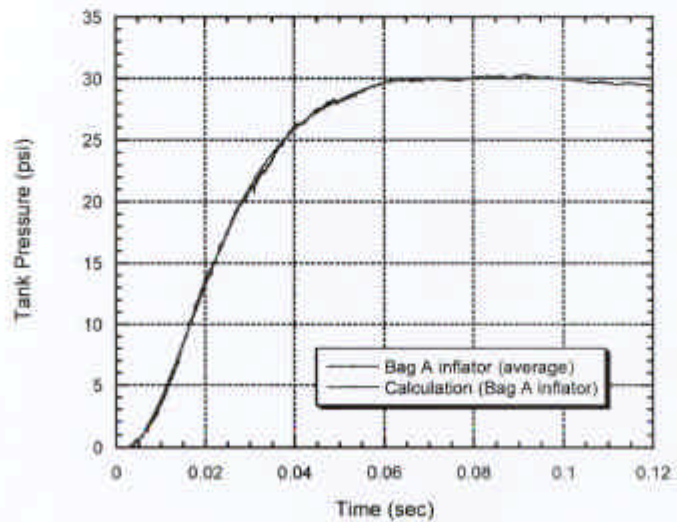


Figure 15. Tank gas pressure data comparison for Bag A inflator.

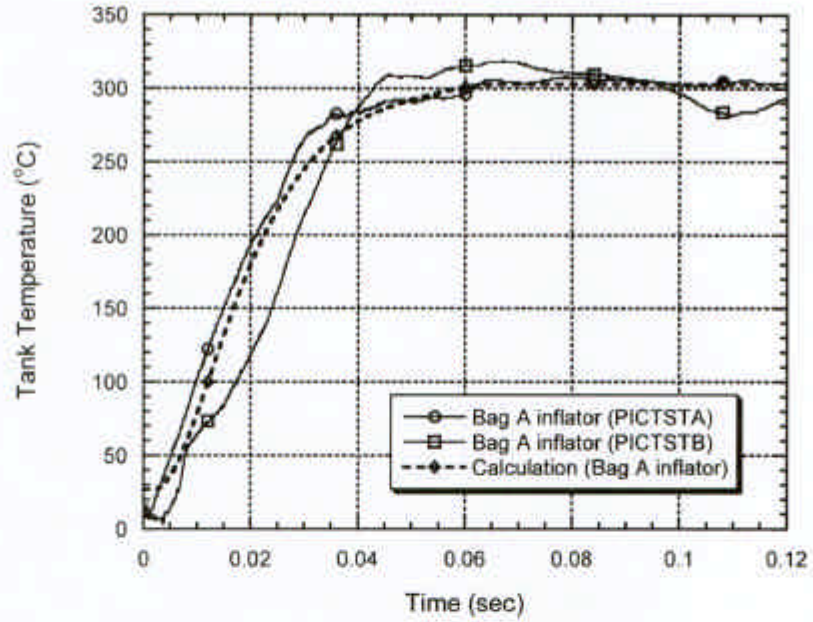


Figure 16. Tank gas temperature data comparison for Bag A inflator.

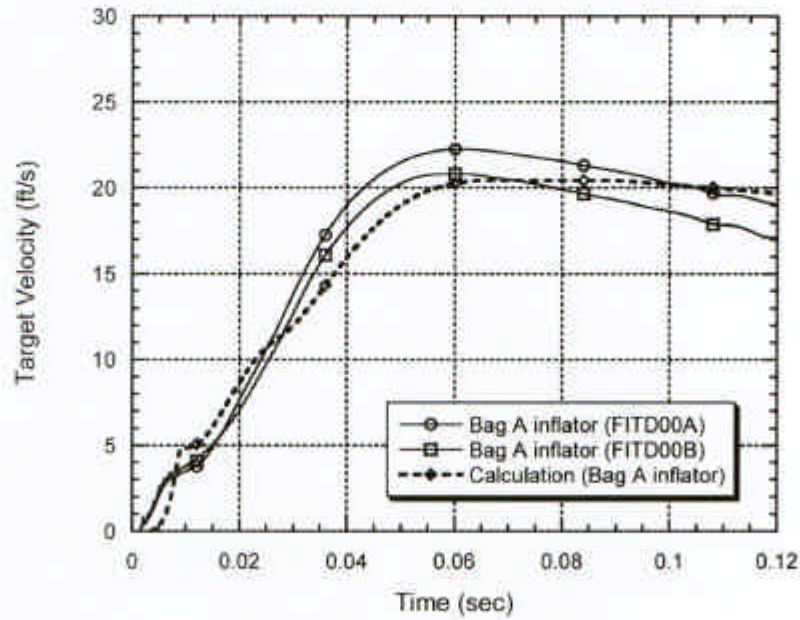


Figure 17. Target velocity data comparison for Bag A inflator.

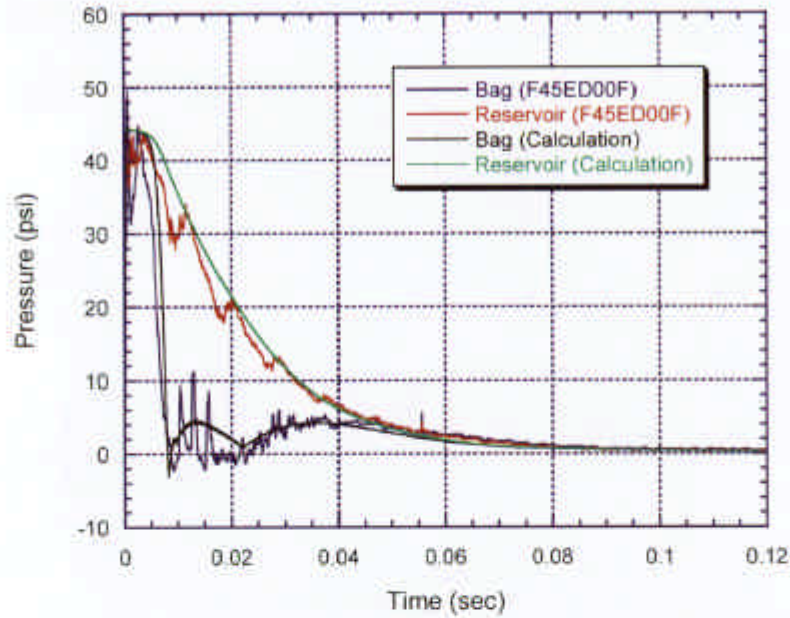


Figure 18. Data comparison of air bag and reservoir pressures for ATS calibration against Bag A inflator.

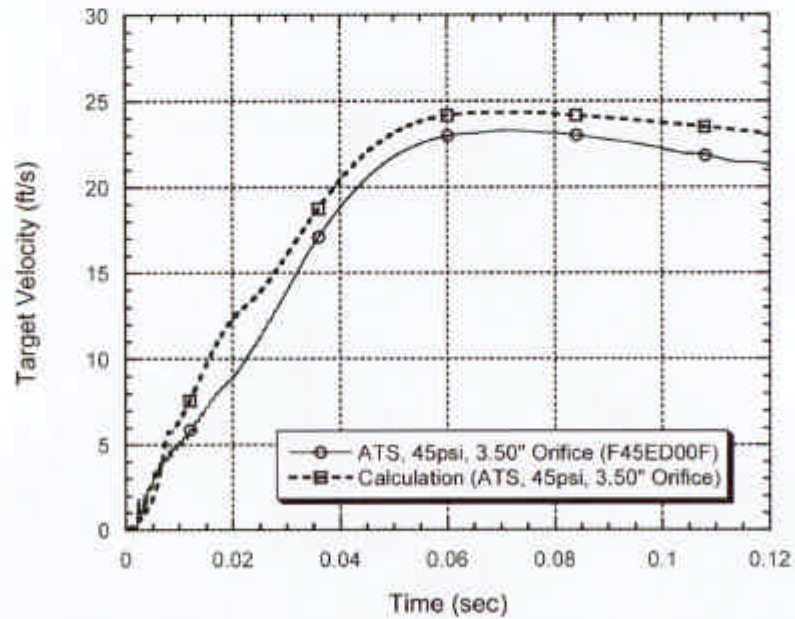


Figure 19. Data comparison of target velocity for ATS calibration against Bag A inflator.

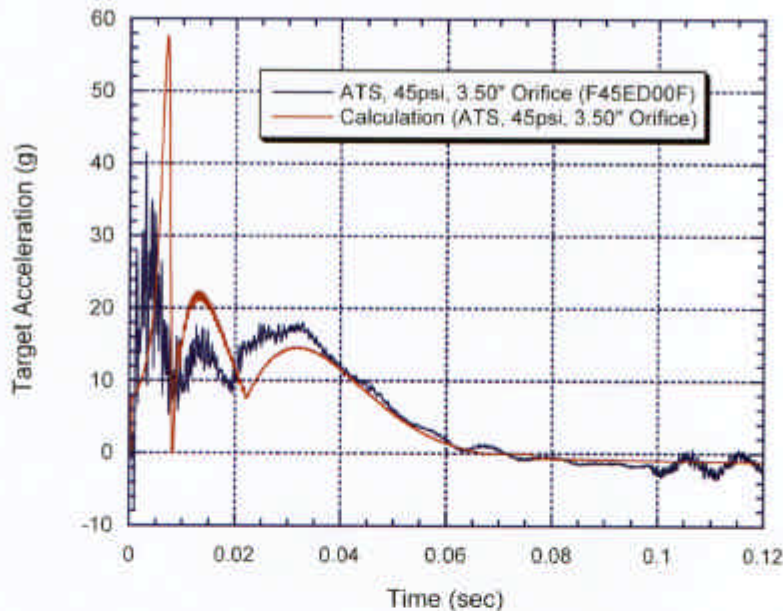
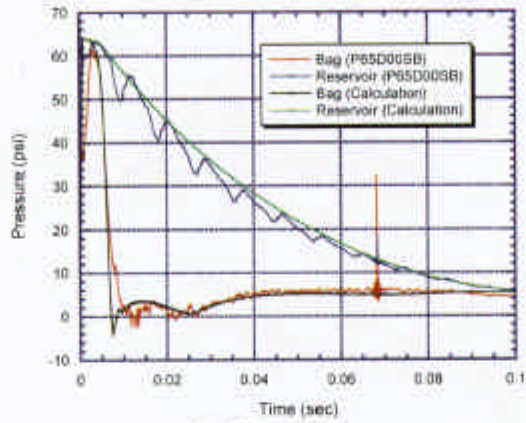


Figure 20. Data comparison of target acceleration for ATS calibration against Bag A inflator.

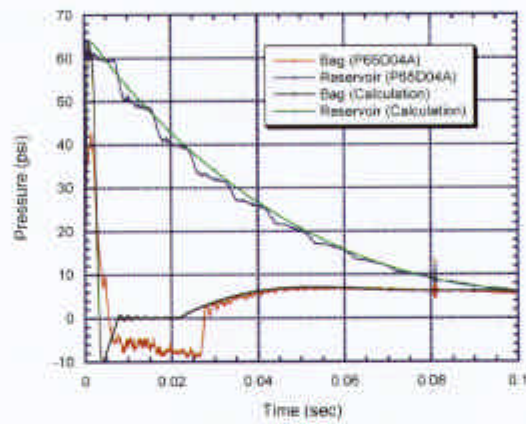
To understand the effects of inflator energy and mass flow rates on air bag-target interaction, parametric calculations were carried out using the model for the Bag A inflator with the target at 0-standoff. Inflator validation results were presented earlier from Figure 15-17. The calculated inflator temperature  $T_i$  for the Bag A inflator is 750 K. Calculations were performed varying the inflator temperature from 500-1500 K for Bag A with and without vent holes, while keeping the total inflator energy output  $E_i$  constant. The inflator mass flow decreases with higher inflator temperature due to reduced gas density as calculated using Eq. (36) (Figure 24).

Calculations show that a change in inflator mass flow only affects the target response when vent holes or leakage are present. For a sealed bag, the calculated target response remains the same independent of the inflator temperature when the energy is held constant (Figure 25). This is expected since equal energy performs equal work if there is no leakage (Figure 25). On the other hand, when leakage is present, the target velocity is lower for higher inflator temperature resulting in lower inflator mass output (Figure 26). Figures 25-26 also show that the vent holes reduce the peak target velocity by about 33%.

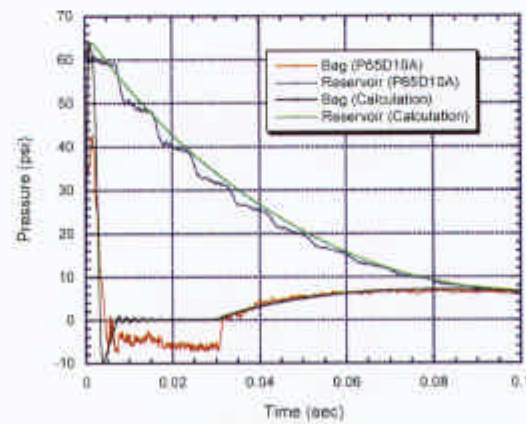
However, a closer comparison between Figs. 25 and 26 show that venting effects on target velocity occur after 20 ms, which seems to suggest that venting may have minimal effect in reducing OOP hazard that is primarily due to the early punch out load before 20 ms. Vent holes seems to primarily affect the membrane load and its effects depend on gas properties.



(a) 0''-standoff

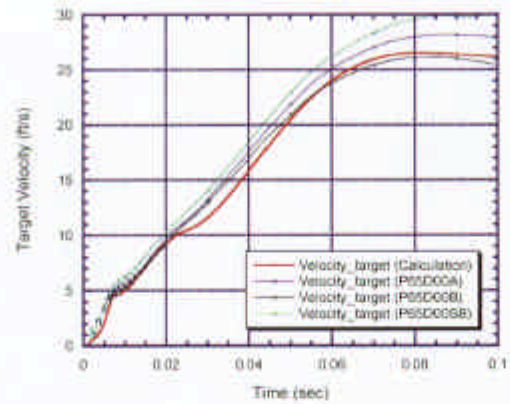


(b) 4''-standoff

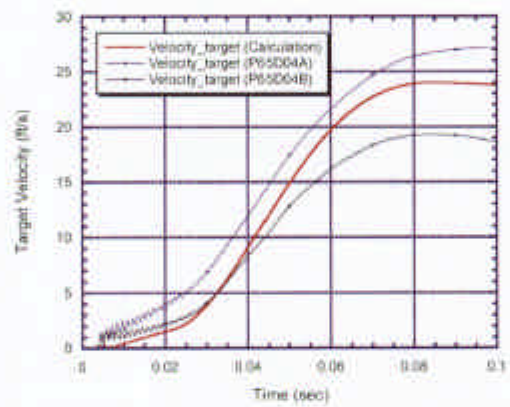


(c) 10''-standoff

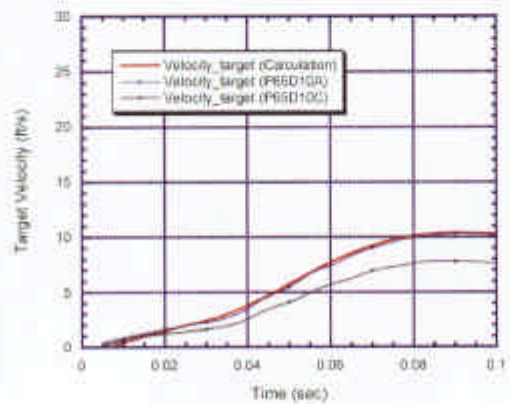
Figure 21. Air bag and reservoir pressure data comparison for proximity tests.



(a) 0''-standoff



(b) 4''-standoff



(c) 10''-standoff

Figure 22. Target velocity data comparison for proximity tests.

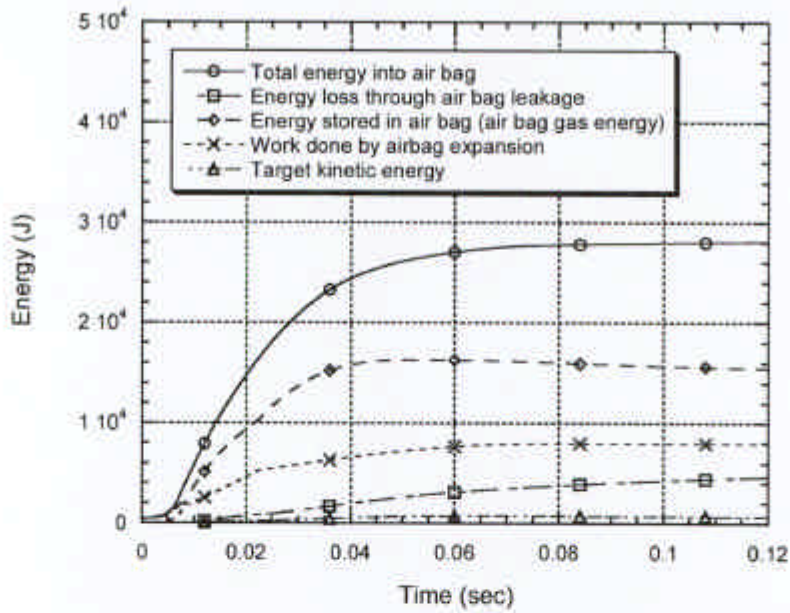


Figure 23. Energy partition during deployment.

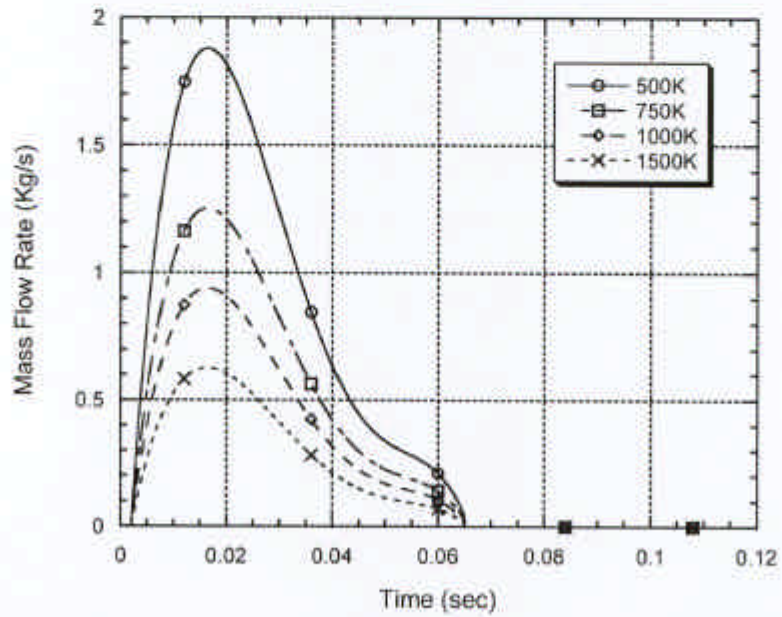


Figure 24. Change of inflator mass flow rate with temperature.

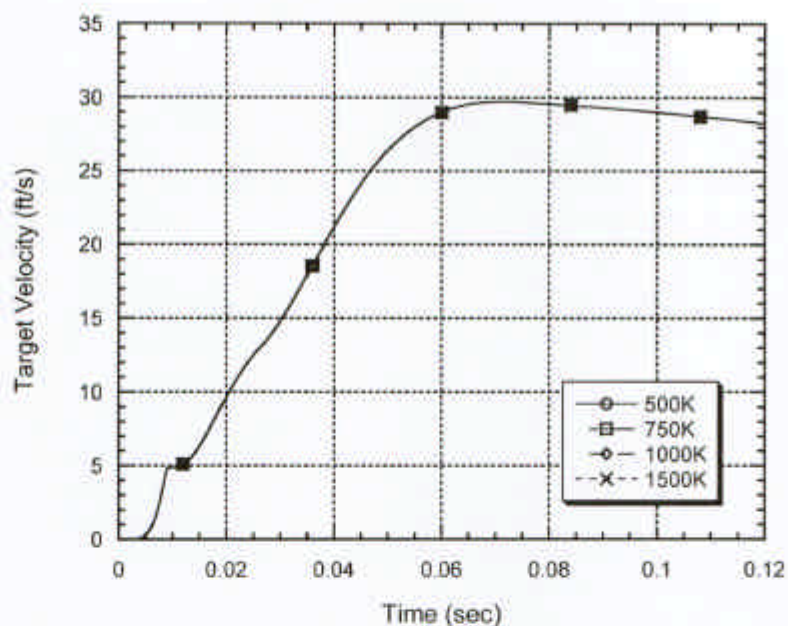


Figure 25. Target velocities for sealed air bag calculated with same inflator energy but different mass flow rates.

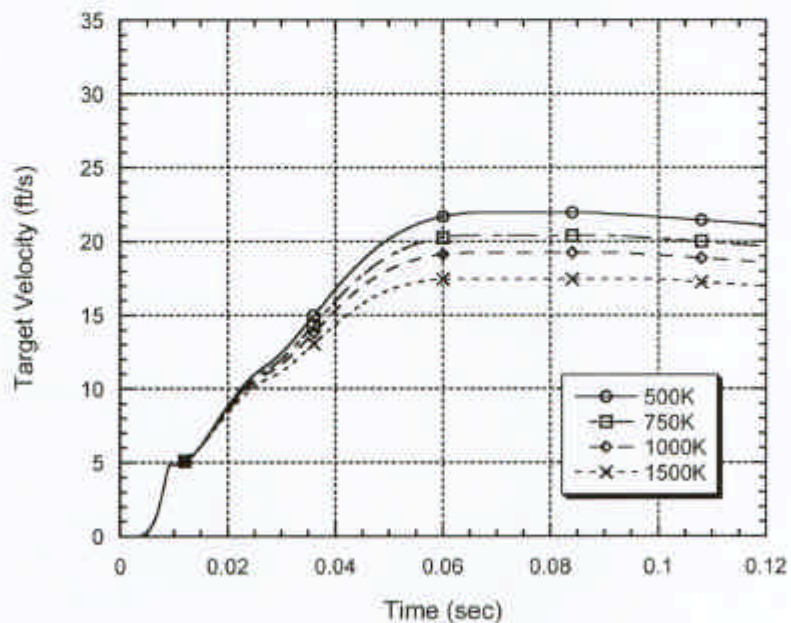


Figure 26. Target velocities for air bag with vent holes and fabric leakage calculated with same inflator energy but different mass flow rates.

## DISCUSSION

An experimental and analytical technique has been developed to study air bag-occupant interaction. An ATS was constructed and was shown calibrate-able against a fleet air bag to adequately replicate target response. One air bag type and used in this study to demonstrate the ATS procedure. The air bag covers were removed for the tests, because although the bag can be reused, the covers can only be ruptured once. The repeated use of a single bag did not appear to have an adverse or systematic effect.

A lumped-parameter analytical model was developed to describe the deployment process of the air bag and its interaction with a rigid target. The integral model relates the volumetric expansion of the bag to the target motion and bag pressure. Although only simple bag volume-area relationships were used, the model captures the observed features of the bag pressures and target responses with favorable data agreement. The model has provided an in-depth phenomenological explanation of the proximity test data on the effects of inflation on the OOP and membrane load trend. The volume-area functions as modeled are semi-empirically based but they address perhaps the least known aspects of bag-target interaction with significant implications on loads delivered to occupants. Only a limited number of cases were simulated for one air bag in the present work. More simulations for a variety of bags will not only refine the bag surface-volume functions but also indicate how such functions change with different air bag designs and deployment conditions, including side air bags.

Some target surface data can be taken to guide understanding, such as using the TekScan surface pressure sensors to measure target surface pressure. Comparison between target surface pressure and bag pressure will help determine more accurately the effects of bag pressure on loading and evaluate the assumption of pressure uniformity during inflation for modeling.

## CONCLUSIONS

A reusable, pneumatic-driven air bag test fixture, the ATS has been constructed to study air bag-occupant interaction and deployment dynamics. Calibration of the ATS against a fleet air bag was demonstrated. The ATS is a research tool for understanding air bag load on occupants in relationship to inflation characteristics. It provides a controlled methodology to evaluate fundamental parameters governing proposed air bag design. The ATS allows the performance of efficient, repeatable deployment tests using the same air bag without the inflator. Benchmark data with quantified error bars can be generated for model and code development validations.

An integral analytical model was developed to analyze the test results to gain phenomenological insight. The parametric calibration of the bag volume-area functions against test data provides a direct understanding of the relatively unknown aspect of bag-target interaction dynamics. The model was validated against both the inflator and ATS test data, including the proximity tests to study standoff effects on target response. Target velocity (and load) decreases with standoff due to the reduction of early inflation pressure pulse, extension of the intermediate expansion, and the slowing down of the final membrane load. Model simulations have helped explain the proximity test results that cannot be easily obtained just from the test data.

Model results have also provided insights on the effects of inflation energy and mass flow on target response. The model results show that only a very small fraction, like 3%, of the total energy is delivered to a target, while 60% is stored inside the bag. For a sealed bag, the target response is independent of inflator temperature if the total energy is held constant. Venting reduces the target load primarily during the final pressurization (membrane) phase. For a vented bag, the target velocity decreases with higher inflator temperature.

## REFERENCES

- CHAN, P.C. and H.H. KLEIN (1994) "A study of blast effects inside an enclosure," *ASME J. Fluids Engrg.*, **116**, pp. 450-455.
- BASS, C. R., CRANDALL, J. R., BOLTON, R. R., PILKEY, W. D., KHAEWPOONG N. and SUN, E. (1999) "Deployment of Air Bags into the Thorax of an Out-of-Position Dummy" SAE Paper 1999-01-0764, *Air Bag Technology 1999*, SAE SP-1411.
- HO, K. H.-H., K. K. KAN, and J. H. STUHMILLER (1997) "A model for the lung injury due to air blast and blunt impact." JAYCOR Technical report J97-2997-05/060.
- HORSCH, J., I. LAU, D. ANDRZEJAK, D. VIANO, J. MELVIN, J. PEARSON, D. COK, and G. MILLER (1990) "Assessment of air bag deployment loads," SAE Paper 902324, International Congress and Exposition, Detroit, Michigan, 1990.
- JOHNSTON, K. L., K. D. KLINICH, D. A. RHULE and R. A. SAUL (1997) "Assessing arm injury potential from deploying air bag," SAE Paper 970400, in "Occupant Protection and Injury Assessment in the Automotive Crash Environment," SP-1231 (SAE, 1997).
- LAU, I. V., J. D. HORSCH, D. C. VIANO, ET AL., (1993) "Mechanism of injury from air bag deployment loads," *Accid. Anal. Prev.* **25**, 29.
- LOBDELL, T. E., K. C. KROELL, D. C. SCHNEIDER, W. E. HERING, and A. M. NAHUM (1972) "Impact response of the human thorax." In Proceeding of the Symposium, "Human Impact Response Measurement and Simulation," General Motors Research Laboratories, Oct. 2-3, 1972, (Plenum Press, New York-London, 1972) 201.
- MELVIN, J. W., J. D. HORSCH, J. D. MCCLEARY, L. C. WIDEMAN, J. L. JENSEN, and M. J. WOLANIN (1993) "Assessment of air bag deployment loads with the small female Hybrid II dummy," in the 37<sup>th</sup> Stapp Car Crash Conference Proceedings, P-269 (SAE, 1993).
- MERTZ, H. J., G. W. NYQUIST, D. A. WEBER, G. D. DRISCOLL, and J. B. LENOX (1995) "Responses of animals exposed to deployment of various passenger inflatable restraint system concepts for a variety of collision severities and animal positions," SAE Paper 826047, in "Biomechanics of Impact Injuries and Injury Tolerances of the Abdomen, Lumbar Spine and Pelvis Complex," edited by S. Backaitis, (SAE, 1995).
- NUSHOLTZ, G. S., WANG, D. and WYLIE, E. B. (1998) "An Evaluation of Air bag Tank-Test Results," SAE Paper 980864, International Congress and Exposition, Detroit, Michigan, Feb. 23-26, 1998, (SAE SP-1320).
- NUSHOLTZ, G. S., WU, J., WANG, D. and WYLIE, E. B. (1999) "Energy and Entropy in Air bag Deployment: The Effect on an Out-of-Position Occupant" SAE Paper No. 1999-01-1071; *Air Bag Technology 1999*, SAE SP-1411.
- PATRICK, L., G. NYQUIST (1972) "Air bag effects on the out-of-position child," Second International Conference on Passive Restraints, 1972, SAE Paper 720442, in "Biomechanics of Impact Injuries and Injury Tolerances of the Abdomen, Lumbar Spine and Pelvis Complex," edited by S. Backaitis, (SAE, 1995).

- PILKEY, W. D., (1996a) "UVA Test Report, OOPS ISO-2 Position Series 1 Tests," prepared for NHTSA, Aug. 24, 1996.
- PILKEY, W. D., (1996b) "UVA Test Report, OOPS ISO-1 Position Series 1 Tests," prepared for NHTSA, Aug. 24, 1996.
- SAE (1995) "Air bag inflator ballistic tank test procedure gas generator used in inflatable restrain systems," SAE J2238.
- SAE (1995) "Driver or passenger Air bag Module Deployment test procedure," SAE J3630, 1995-03.
- STUHMILLER, J. H., K. H. HO, M. J. VANDER VORST, K. T. DODD, T. FITZPATRICK, and M. MAYORGA (1996) "A model of blast overpressure injury to the lung." *J. Biomechanics*, **29**, 222.
- SULLIVAN, L. K., J. M. KOSSAR (1992) "Air bag deployment characteristics," National Highway Traffic Safety Administration Report No. DOT HS 807 869, February, 1992.
- TANAVDE, A. S., K. GUDIPATY, and S. VALDYARAMAN (1997) "Simulation of seat integrated side air bag deployment," SAE Paper 970127, in "Occupant protection and injury assessment in the automotive crash environment," SP-1231 (SAE, 1997).
- VIANO, D. C., and I. V. LAU (1988) "A viscous tolerance criterion for soft tissue injury assessment." *J. Biomechanics*, **21**, 387.
- WAWA, C. J., J. S. CHANDRA, and M. K. VERMA (1993) "Implementation and validation of a finite element approach to simulate occupant crashes with air bags: Part I – air bag model." in "Crashworthiness and occupant protection in transportation systems," *AMD-Vol. 169/BED-Vol. 25 (ASME, 1993)*.
- YOGANANDAN, N., F. A. PINTAR, D. SKRADE, W. CHMIEL, J. M. REINARTZ, and A. SANCES, JR. (1993) "Thoracic biomechanics with air bag restraint," SAE Paper 933121, in the *37<sup>th</sup> Stapp Car Crash Conference Proceedings, P-269 (SAE, 1993)*.

## APPENDIX A

In Figure A-1, we show an air bag in a general shape with surface area  $A(t)$  at time  $t$ . It touches the target with a contact area  $A_C$ . At time  $t + \Delta t$ , the bag expands to the surface  $A(t + \Delta t)$  and the area in contact with the target is  $A_C(t + \Delta t)$ . We divide the bag into small elements  $ds$ . As the bag expands the elements expand with uniform proportion and the dash lines in Figure A-1 represent the trajectories of the elements as they expand from  $t$  to  $t + \Delta t$ . Note that  $A_C$  expands to  $A_C'$  which is different from  $A_C(t + \Delta t)$ , in general. In finite difference form, the equation for the normal motion of the free element  $ds$  can be written as

$$\lim_{\Delta t \rightarrow 0} \frac{1}{\Delta t} \left\{ [v_n \sigma ds]_{t+\Delta t} - [v_n \sigma ds]_t \right\} = (P_B - P_A) ds. \quad (\text{A-1})$$

To obtain the bag equation, Eq. (10), we need to sum up (A-1) over all of the free elements. The free elements at time  $t$  are shown in Figure A-1 in the shaded area and we have

$$\sum_{\text{shaded area}} = \sum_{\text{whole bag}} - \sum_{\text{unshaded area}}. \quad (\text{A-2})$$

The summation of the left-handed side of (A-1) over the whole bag leads to

$$\begin{aligned} \sum_{\text{whole bag}} &\equiv \lim_{\Delta t \rightarrow 0} \frac{1}{\Delta t} \left\{ \sum_{\text{whole bag}} [v_n \sigma ds]_{t+\Delta t} - \sum_{\text{whole bag}} [v_n \sigma ds]_t \right\} \\ &= \frac{d}{dt} \int_{\text{whole bag}} [v_n \sigma ds] \\ &= \frac{d}{dt} \left( \sigma \frac{dV}{dt} \right). \end{aligned} \quad (\text{A-3})$$

For the unshaded area, we have

$$\sum_{\text{unshaded area}} \equiv \lim_{\Delta t \rightarrow 0} \frac{1}{\Delta t} \left\{ \sum_{\text{unshaded area}} [v_n \sigma ds]_{t+\Delta t} - \sum_{\text{unshaded area}} [v_n \sigma ds]_t \right\}. \quad (\text{A-4})$$

Since the unshaded area at time  $t$  is  $A_C$ , the second sum in the right-handed side of (A-4) is

$$\sum_{\text{unshaded area}} [v_n \sigma ds]_t = [\dot{x}_C \sigma A_C]_t. \quad (\text{A-5})$$

On the other hand, the first sum in the right-handed side of (A-4) is

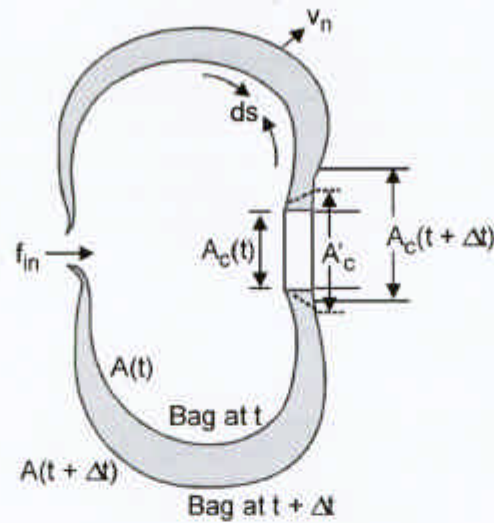


Figure A-1. Schematic of air bag expansion.

$$\begin{aligned}
 \sum_{\text{unshaded area}} [v_n \sigma ds]_{t+\Delta t} &= \int_{A'_c} [v_n \sigma ds]_{t+\Delta t} \\
 &= \int_{A_c(t+\Delta t)} [v_n \sigma ds]_{t+\Delta t} + \int_{A'_c - A_c(t+\Delta t)} [v_n \sigma ds]_{t+\Delta t} \\
 &= [\dot{x}_c \sigma A_c]_{t+\Delta t} + \int_{A'_c - A_c(t+\Delta t)} [v_n \sigma ds]_{t+\Delta t}.
 \end{aligned} \tag{A-6}$$

Regarding  $v_n$  as a function of space and time, we expand  $v_n(t + \Delta t)$  around the edge of  $A_c(t + \Delta t)$  as

$$\begin{aligned}
 v_n(\vec{r}, t + \Delta t) &\approx v_n(\vec{r}_c, t + \Delta t) + \nabla v_n(\vec{r}_c, t + \Delta t) \cdot \Delta \vec{r}_c \\
 &= \dot{x}_c + \nabla v_n(\vec{r}_c, t + \Delta t) \cdot \Delta \vec{r}_c,
 \end{aligned} \tag{A-7}$$

where  $\Delta \vec{r}_c$  is the distance vector connecting the point of integration from the nearest point at the boundary of  $A_c(t + \Delta t)$ . Then,

$$\begin{aligned}
 \int_{A'_c - A_c(t+\Delta t)} [v_n \sigma ds]_{t+\Delta t} &= \int_{A'_c - A_c(t+\Delta t)} [(\dot{x}_c + \nabla v_n(\vec{r}_c, t + \Delta t) \cdot \Delta \vec{r}_c) \sigma ds]_{t+\Delta t} \\
 &= [\dot{x}_c \sigma]_{t+\Delta t} A'_c - [\dot{x}_c \sigma A_c]_{t+\Delta t} + \int_{\Gamma_c} \nabla v_n(\vec{r}_c, t + \Delta t) \cdot \Delta \vec{r}_c \sigma \Delta r_c d\Gamma,
 \end{aligned} \tag{A-8}$$

where  $\Gamma$  is the boundary of  $A_c(t + \Delta t)$  and  $\Delta r_c$  is the width of band  $A'_c - A_c(t + \Delta t)$ . By the assumption of uniform stretch,

$$\sigma(t + \Delta t)A'_c = \sigma(t)A_c(t). \quad (\text{A-9})$$

Collecting the results of Eqs. (A-5), (A-6), (A-8) and (A-9) in (A-4), we have

$$\begin{aligned} \sum_{\text{unshaded area}} &\equiv \lim_{\Delta t \rightarrow 0} \frac{1}{\Delta t} \left\{ \left[ \dot{x}_c(t + \Delta t) - \dot{x}_c \right] \sigma(t) A_c(t) + (\Delta t)^2 \int_{\Gamma_c} \nabla v_n \cdot \frac{\Delta \vec{r}_c}{\Delta t} \sigma \frac{\Delta r_c}{\Delta t} d\Gamma \right\} \\ &= \sigma A_c \ddot{x}_c + \lim_{\Delta t \rightarrow 0} \Delta t \int_{\Gamma_c} \nabla v_n \cdot \frac{d\vec{r}_c}{dt} \sigma \frac{dr_c}{dt} d\Gamma. \end{aligned} \quad (\text{A-10})$$

The second term in the second line of (A-10) goes to zero as  $\Delta t \rightarrow 0$ , since the integral is finite. The final equation for the bag is then

$$\frac{d}{dt} \left( \sigma \frac{dV}{dt} \right) - \sigma A_c \ddot{x}_c = (A - A_c)(P_B - P_A). \quad (\text{A-11})$$

